International Journal of Nanomedicine

Dovepress
Taylor & Francis Group

Open Access Full Text Article

ORIGINAL RESEARCH

Platelet Membrane-Coated Poly (Lactic-Co-Glycolic Acid) Nanoparticles as a Targeting Drug Delivery System for Multidrug-Resistant Breast Cancer

Bomin Song[1,*], Young-Guk Na[1,*], Byung Jin Kim[1,*], Minki Jin[1], Yo Han Song[1], Da-Eun Kim[1], Suyeon Hwang[1], Jong-Suep Baek[2], Hong-Ki Lee[3], Cheong-Weon Cho[1]

[1]College of Pharmacy, Chungnam National University, Daejeon, 31434, Republic of Korea; [2]Department of Bio-Health Convergence, Kangwon National University, Chuncheon, 24341, Republic of Korea; [3]College of Veterinary Medicine, Chungbuk National University, Chungbuk, 28644, Republic of Korea

*These authors contributed equally to this work

Correspondence: Cheong-Weon Cho; Hong-Ki Lee, Email chocw@cnu.ac.kr; hongki.lee@cbnu.ac.kr

Introduction: Paclitaxel (PTX), widely used chemotherapeutic agent, is limited by poor solubility, P-glycoprotein (P-gp) mediated efflux, and non-specific toxicity. To overcome these challenges, we developed a triple-functionalized nanocarrier system incorporating poly(lactide-co-glycolide) (PLGA)-based nanoparticles (PNs), D-α-tocopheryl polyethylene glycol succinate (TPGS) for P-gp inhibition, and platelet membrane (PM) coating for targeted tumor delivery.

Methods: The PM-coated TPGS-modified PNs with PTX (PTPNs) was characterized by particle size analysis, transmission electron microscopy (TEM), and protein assay to confirm PM coating. In vitro drug release studies were conducted under acidic conditions mimicking the tumor microenvironment. Cellular assays were performed to evaluate cytotoxicity and drug efficacy in multidrug-resistant MCF-7/ADR cells. In vivo biodistribution and xenograft studies assessed tumor accumulation and therapeutic outcomes.

Results: PTPNs exhibited a particle size of 221 ± 2 nm with a PDI of 0.090 ± 0.020 and a zeta potential of –30.5 ± 0.3 mV, indicating a homogeneous particle distribution and successful PM coating. The optimal PM-to-PLGA weight ratio was determined to be 0.005, which ensured structural stability and uniform coating in physiological conditions. Sustained PTX release was observed in acidic conditions, mimicking the tumor microenvironment. Cellular assays showed a 17-fold reduction in PTX IC_{50} in MCF-7/ADR cells compared to free PTX, attributed to the synergistic effects of TPGS-mediated P-gp inhibition and PM–based tumor targeting. In vivo, PTPNs demonstrated enhanced tumor accumulation and significantly reduced tumor burden, with final tumor volume 2.6-fold lower than that of TPNs and 3.6-fold lower than that of the PTX commercial product (Taxol®)-treated group. Tumor necrosis factor-α (TNF-α) levels were also reduced, reflecting decreased tumor-promoting cytokine activity.

Conclusion: The PTPNs enhanced PTX delivery by improving tumor specificity, overcoming multidrug resistance, and reducing systemic toxicity. These results suggested the potential of this biomimetic approach to advance cancer therapy.

Keywords: paclitaxel, platelet membrane, Poly(lactide-co-glycolide), nanoparticles, multidrug resistance, cancer therapy

Introduction

Paclitaxel (PTX) is a widely used chemotherapeutic agent for the treatment of breast and ovarian cancers. Its mechanism of action involves stabilizing tubulin polymerization into microtubules and inhibiting their depolymerization, which halts the cell cycle at the G2/M phase, ultimately inducing cancer cell death.[1,2] Despite its therapeutic efficacy, PTX suffers from low aqueous solubility, poor membrane permeability, and susceptibility to P-glycoprotein (P-gp)-mediated efflux, leading to multidrug resistance and reduced efficacy.[3,4] To improve its solubility, commercial formulations such as Taxol® (PTX commercial product) solubilize PTX using Cremophor EL, but this excipient is associated with severe

Received: 13 February 2025
Accepted: 23 June 2025
Published: 2 July 2025

hypersensitivity reactions, nephrotoxicity, and neurotoxicity, requiring premedication, and limiting patient compliance.[5] Although alternative formulations such as Abraxane® (albumin-bound PTX) and Genexol-PM® (polymeric micelle-based PTX) have been developed to overcome some limitations. However, these systems are limited by micelle instability and poor tumor targeting, which can result in premature drug release, non-specific distribution, and systemic side effects.[6]

Nanoparticles based on poly(lactide-co-glycolide) (PLGA), a biodegradable and biocompatible polymer, offer a promising approach to overcoming limitations of PTX.[7,8] PLGA nanoparticles (PNs) can encapsulate hydrophobic drugs like PTX, enhance solubility, and provide controlled drug release. Furthermore, by adjusting parameters such as molecular weight and the lactide-to-glycolide ratio, PLGA system can be tailored to achieve specific drug release profiles, improving therapeutic outcomes.[9] Despite these advantages, conventional PNs faces significant challenges, including rapid opsonization and immune clearance due to their hydrophobic surfaces and negative charges.[10] This can lead to premature removal by the mononuclear phagocytes system and non-specific distribution, increasing systemic toxicity and reducing drug delivery efficiency.[11]

To overcome these challenges, nanoparticle surface modifications have been investigated to improve colloidal stability and reduce premature clearance by the mononuclear phagocyte system (MPS), thereby limiting non-specific distribution. D-α-tocopherol polyethylene glycol succinate (TPGS), an amphiphilic molecule, has been widely studied as both a stabilizer and a P-gp inhibitor.[12] TPGS enhances the colloidal stability of PLGA nanoparticles and inhibits P-gp–mediated drug efflux, thereby promoting intracellular drug retention and reducing multidrug resistance.[13] In addition, its PEG moiety contributes to reduced opsonization and MPS uptake, which helps prolong systemic circulation. TPGS-modified PLGA nanoparticles loaded with PTX (TPNs) offer dual benefits: improved absorption and resistance modulation.[14] However, while TPGS improves nanoparticle stability and reduces systemic clearance, it does not inherently confer tumor specificity.

To achieve tumor-targeted delivery, platelet membrane (PM) coating has been applied as a biomimetic strategy.[15,16] PM-coated nanoparticles combine the natural properties of PM with the controlled delivery capabilities of synthetic nanoparticles. The PM contains surface protein such as integrins and glycoproteins that aid in immune evasion and targeted delivery.[17] Specifically, P-selectin, a glycoprotein present on PM, binds to CD44 receptors overexpressed in several tumors, enabling selective accumulation of the nanoparticles at the tumor site.[18] This strategy not only enhances circulation time but also minimizes off-target effects, reducing toxicity to healthy tissues.[19,20]

The goal of this study was to develop PM-coated TPGS-modified PNs loaded with PTX (PTPNs) as a novel PTX delivery system to enhance solubility, inhibit P-gp-mediated efflux, and achieve tumor-specific targeting (Figure 1). The physicochemical properties of PTPNs were characterized, and their cellular uptake, cytotoxicity, biodistribution, and therapeutic efficacy were evaluated through in vitro and in vivo studies. By combining the advantages of PLGA, TPGS, and PM coating, PTPNs offer a multifaceted approach to overcoming the limitations of conventional PTX formulations and improving outcomes in cancer therapy.

Experimental Section

Materials

PTX was supplied by Korea United Pharm Inc (Seoul, Republic of Korea). PLGA (Resomer RG 502H: 50:50 lactic acid: glycolic acid, -COOH end groups) was purchased from Evonik Industries (Essen, Germany). Dichloromethane (DCM), dimethyl sulfoxide (DMSO) and formic acid (FA) were purchased from Samchun Chemical (Pyungtaek, Republic of Korea). High-performance liquid chromatography (HPLC) grade acetonitrile and methanol were purchased from J.T Baker (Philipsburg, NJ, USA). Polyvinyl alcohol (PVA; 87–90% hydrolyzed, average molecular weight 30,000–70,000), TPGS, 3-(4,5-dimethylthiazol-2yl)-2,5-diphenyl-2H-tetrazolium bromide (MTT), coumarin 6 (C6) were purchased from Sigma-Aldrich (St. Louis, MO, USA). Pierce protease inhibitor mini tablets, Pierce BCA protein assay kits, Hoechst 33342 solution (20 mmol), Pierce CN/DAB Substrate Kit, and NuPAGE LDS Sample Buffer (4X) were purchased from ThermoFisher (Wilmington, DE, USA). Cyanine5.5 NHS ester (Cy5.5) was purchased from Lumiprobe (Hunt Valley,

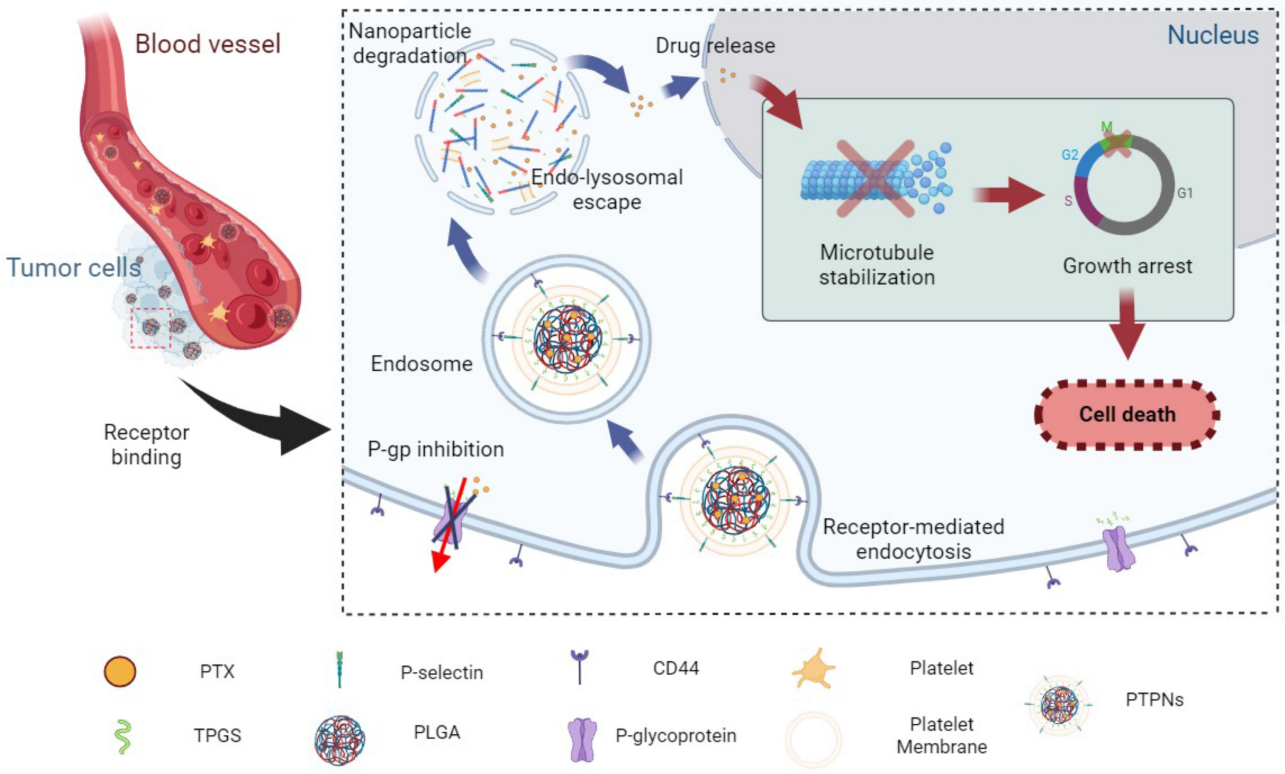

Figure 1 PM-coated TPGS-modified PLGA nanoparticles loaded with PTX (PTPN) designed for the treatment of multidrug-resistant breast cancer. The mechanism involves selective targeting of tumor cells via P-selectin on the PM binding to CD44 receptors overexpressed on cancer cells. Following receptor-mediated endocytosis, the nanoparticles escape the endo-lysosomal pathway and release PTX in the acidic tumor microenvironment, stabilizing microtubules and inducing apoptosis.

MD, USA). Dulbecco's modified Eagle's medium (DMEM), fetal bovine serum (FBS), penicillin-streptomycin, and trypsin-EDTA were provided from Gibco BRL (Gaithersburg, MD, USA).

Preparation of TPNs

TPNs was optimized with Box-behnken design (Supporting Information 1) and prepared as follows.[21] Briefly, PTX (5 mg) and PLGA (116.4 mg) was dissolved in DCM (5 mL). The oil phase was then added into distilled water (DW; 25 mL) containing PVA (1 w/v%) and TPGS (0.082 w/v%). Emulsification was performed using a Vibra-Cell probe sonicator (Sonics & Material Inc., Newtown, CT, USA) at an amplitude 150 W with 5:1 on/off cycle for 4.5 min. To remove the organic solvent, the oil-in-water emulsion was stirred overnight, resulting in a suspension. The suspension was then centrifuged at 21,206 g for 10 min at 10°C. After centrifugation, the supernatant was discarded, and DW was added to resuspend the nanoparticles. Additionally, TPNs without PTX (B-TPNs), C6-loaded TPNs (C6-TPNs), and Cy5.5-loaded TPNs (Cy5.5-TPNs) were prepared using the same procedure. The TPNs was characterized based on particle size, zeta potential, polydispersity index (PDI), encapsulation efficiency (EE), scanning electron microscopy (SEM), and transmission electron microscopy (TEM) analysis, as detailed in the Supporting Information 1.

Preparation of PTPNs

Fabrication of PTPNs with PM and TPNs

TPNs and PM were fused using a sonication method.[22] For PM purification, whole blood was collected from rats into EDTA-containing Vacutainer blood collection tube (Becton Dickinson, Franklin Lakes, NJ, USA). The blood was centrifuged at 100 g for 20 min at room temperature twice to separate red blood cells and white blood cells. Platelet rich plasma (PRP) was then isolated, and phosphate buffer saline (PBS) containing EDTA (1 mmol), prostaglandin E1 (2 μmol), and a protease inhibitor was added to the PRP. The resulting PRP was pelleted twice by centrifugation at 800 g for 20 min at room temperature (RT) and resuspended in PBS. To prepare PM, the PRP was subjected to three freeze—

thaw cycles by freezing at −80°C and thawing at RT. The processed PRP was then pelleted and then centrifuged at 100 g for 20 min twice at RT to separate by centrifugation at 4000 g for 3 min. The resulting PRP pellet, identified as the PM, was resuspended in PBS, and sonicated for 5 min using a batch sonicator operating at a frequency of 42 kHz and a power of 100 W. For the fusion process, TPNs and PM suspensions were mixed and further sonicated under the same conditions (42 kHz, 100 W) for 3 min. The fused nanoparticles (PTPNs) were then purified by centrifugation at 21,206 g for 10 min using the same procedure, PTPNs without PTX (B-PTPNs), C6-loaded PTPNs (C6-PTPNs), and Cy5.5-loaded PTPNs (Cy5.5-PTPNs) were also prepared.

Optimization of PM/PLGA Ratios Within PTPNs

The optimal PM to PLGA (PM/PLGA) ratio (w/w) for PTPNs was determined based on particle size changes after adjustment in PBS or plasma.[23] Various PTPNs were prepared with varying PM/PLGA ratios ranging from 0.00125 to 0.02. The PM content was quantified using the Pierce BCA assay kit. Following synthesis, the PTPNs were adjusted with PBS or plasma, and their particle size was measured as described in the Supporting Information 1. During the adjustment process, PTPN pellets were collected by centrifugation at 21,206 g for 10 min at 10°C, and the supernatant was discarded. The resulting pellets were redispersed in PBS or plasma. The coated structure of PTPNs was confirmed via TEM as detailed in the Supporting Information 1. The optimal PM/PLGA ratio was selected based on particle size changes and TEM imaging results.

Characterization of PTPNs

Particle Size and Morphology

The PTPNs was characterized based on particle size, PDI, zeta potential, and TEM, as detailed in the Supporting Information 1 (n=3).

Western Blot for CD41 Antigen

PM, PTPNs and bovine serum albumin (BSA) were normalized to equivalent total protein concentration using Pierce BCA protein assay kits. Western blotting was performed to confirm the presence of the CD41 antigen, a platelet-specific protein marker.[24] Samples were prepared in LDS sample loading buffer, heated to 70°C for 10 min, and subsequently loaded onto a 10% polyacrylamide gel. Protein separation was carried out at 100 V for 90 min. Following electrophoresis, the samples were transferred onto a polyvinylidene difluoride (PVDF) membrane at 80 V for 180 min. The membranes were blocked with BSA (5 w/v%) at room temperature for 1 h and then incubated overnight at 4°C with a primary integrin αIIb horseradish peroxidase (HRP) antibody (1:1000 dilution; Santa Cruz Biotechnology, Inc., Dallas, TX, USA). The membranes were subsequently incubated with a secondary mouse IgG Fc binding protein conjugated to HRP antibody (1:1000 dilution; Santa Cruz Biotechnology, Inc., Dallas, TX, USA) at room temperature for 1 h. Protein bands were visualized using the Pierce CN/DAB Substrate kit.

In vitro Release of PTX

The cumulative drug release of PTX from TPNs and PTPNs was evaluated under controlled conditions.[25] Briefly, centrifuged pellets obtained from TPNs and PTPNs suspension (2 mL) were transferred into microcentrifuge tubes and dispersed in buffer (1 mL). The tubes were placed in a shaking water bath at 100 rpm and maintained at 37°C. At predetermined time intervals, the samples were centrifugated at 21,206 g for 10 min at 10°C. An aliquot of the supernatant (100 μL) was collected and replaced with an equal volume of fresh buffer to maintain sink conditions. The buffers used were pH 4.5, 6.8, and 7.4, supplemented with sodium dodecyl sulfate (2% w/v). All experiments were performed in 3 replicates (n=3). Sampling was performed over 96 h, and the PTX concentrations were quantified using a liquid chromatography-tandem mass spectrometry (LC-MS/MS) system in Supporting Information 2.

Cell Study

Cell Culture

Human breast cancer cell (MCF-7) and breast cancer resistance cells (MCF-7/ADR) were obtained from the Korean Cell Line Bank (Seoul, Republic of Korea). Both MCF-7 and MCF-7/ADR cells were cultured in DMEM supplemented with FBS (10 v/v%) and penicillin-streptomycin (1% v/v). The cells were maintained in 5% CO_2 incubator at 37°C.

Cell Viability Study

MCF-7 and MCF-7/ADR cells were seeded at a density of 3×10^4 cells per well in a 96-well plate and incubated for 24 h under 5% CO_2 at 37°C. Free PTX, B-TPNs, B-PTPNs, TPNs, and PTPNs were diluted with DMEM to achieve various PTX concentrations. Following incubation for 24 h and 48 h, 30 μL of MTT solution (5 mg/mL) was added to each well, and the plates were incubated for an additional 3 h. After incubation, the medium was carefully removed, and DMSO (200 μL) was added to dissolve the formazan crystals. Absorbance was measured at 565 nm using a microplate reader (Multiskan skyhigh, ThermoFisher Scientific, Waltham, MA, USA).[25] Cell viability was calculated using the following equation:

$$\text{Cell viability}(\%) = \frac{\text{OD}_{\text{sample}}}{\text{OD}_{\text{control}}} \times 100$$

In this equation, $\text{OD}_{\text{sample}}$ represents the absorbance value of cells treated with test formulations, while $\text{OD}_{\text{control}}$ corresponds to the absorbance value of cells cultured in DMEM alone. All experiments were performed in 5 replicates (n=5).

Flow Cytometry

The cellular uptake of C6 from free C6, C6-TPN, and C6-PTPNs in MCF-7 and MCF-7/ADR cells was evaluated.[16] MCF-7 and MCF-7/ADR cells were seeded in 6-well plates at a density of 3×10^4 cells/well in medium (2 mL) and cultured in a CO_2 incubator for 24 h. Following incubation, the medium in each well was removed, and the cells were washed with PBS. Subsequently, 2 mL of free C6, C6-TPNs, or C6-PTPNs (200 ng/mL in DMEM) was added to the wells, and the cells were incubated for 2, 6, and 24 h. After the designated incubation times, the cells were harvested, and a fluorescence assay was performed (n = 3). Fluorescence quantification of C6 uptake from free C6, C6-TPNs, and C6-PTPNs was analyzed using flow cytometry (FACS Canto II, Becton Dickinson, Franklin Lakes, NJ, USA).

In vivo Evaluation

Animals and Tumor Model

Female BALB/c nude mice (Orient, Seoul, Republic of Korea) were housed under standard conditions in a light-controlled room at 22°C. The xenograft model was established by subcutaneously injecting 5×10^6 MCF-7/ADR cells suspended in 50% Matrigel Matrix solution (Corning, Tewksbury, MA, USA) in PBS into the right flank of the mice.[26] Prior to cell injection, mice were pretreated with 3 mg/kg of 17β-estradiol (Sigma-Aldrich, St. Louis, MO, USA) two weeks in advance.[27] All animal experiments were approved by the Local Ethical Committee of Chungnam National University (Approval No. 202310A-CNU-193) and conducted in accordance with the guidelines established by the Chungnam National University Institutional Animal Care and Use Committee (Daejeon, Republic of Korea).

Biodistribution Assay

To evaluate the dynamic distribution of the formulations, PTX was replaced with the fluorescent probe Cy5.5.[28] When the tumor volume reached approximately 100 mm^3, nude mice were randomly divided into four groups (n=3): free Cy5.5, Cy5.5-TPNs, and Cy5.5-PTPNs. The formulations were dispersed in distilled water by sonication and administered intravenously at a dose of 0.01 mg/kg of Cy5.5. Fluorescence intensity was monitored using the VISQUE In Vivo Smart-LF (Vieworks, Anyang, Republic of Korea) at 2, 4, 6, 12, and 24 h post-injection.[26] After 24 h, the mice were sacrificed, and major organs (liver, heart, spleen, kidney, and lungs) as well as the tumor tissue were excised for fluorescence imaging. Fluorescence intensities were measured at an excitation wavelength of 630–680 nm and an emission wavelength of 690–740 nm.

Antitumor Activity Study

The antitumor efficacy of the formulations was evaluated in a xenograft mouse model.[26] Mice were intravenously administrated with PBS, PTX commercial product, TPNs, or PTPNs, each dispersed in distilled water by sonication, once every three days at a PTX dose of 5 mg/kg. Tumor length and width were measured using a Vernier caliper, and tumor volume was calculated using the following equation: Tumor volume = 0.5 × length (mm) × [width (mm^2)]^2. Once the

tumor volume exceeded 100 mm^2, the mice were randomly divided into four groups (n = 5). Tumor volume and body weight were monitored daily throughout the experiment. On day 14, the mice were sacrificed, and blood and tumor tissues were collected. Tumor tissues were weighed and photographed for analysis.

Blood samples were centrifuged to obtain serum, and enzyme-linked immunosorbent assay (ELISA) was performed to quantify tumor necrosis factor-α (TNF-α) levels, a cytokine related to tumor immunity, using a Mouse TNF-α ELISA kit (Invitrogen Life Technologies, Gaithersburg, MD, USA). (n=5).[29]

Statistical Analysis

All results are presented as mean ± standard deviation (SD). Statistical significance between groups was determined using one-way analysis of variance (ANOVA) and two-way ANOVA, followed by pairwise comparisons using the Student's *t*-test. Differences were considered statistically significant at $p < 0.05$, with significance levels indicated as follows: $*p < 0.05$, $**p < 0.01$, $***p < 0.001$, and $****p < 0.0001$.

Results and Discussion

Characterization of TPNs

The physicochemical properties of TPNs were evaluated to confirm their suitability as a PTX delivery system. The optimized TPNs exhibited a particle size of 208 ± 6 nm and a PDI of 0.087 ± 0.014, indicating uniform size distribution. These results are considered appropriate for nanoparticle intended for systemic drug delivery, as particles in this size range are known to enhance circulation time and tumor accumulation via the enhanced permeability and retention effect.[30] The EE of PTX in TPNs was measure as 68.9 ± 2.4%, demonstrating the effectiveness of the PLGA matrix in encapsulating hydrophobic drugs such as PTX. This high EE is attributed to the properties of PLGA, which can accommodate hydrophobic drugs, and the inclusion of TPGS, which enhances encapsulation by reducing interfacial tension during the emulsification process.[31]

Morphological analysis using SEM and TEM confirmed that TPNs was spherical and had smooth surfaces (Figure 2a and b). The particle size observed in the images was consistent with dynamic light scattering measurements, supporting their uniformity and stability. Such structural integrity is critical for achieving predictable drug release and stability under physiological conditions.[32] These findings established TPNs as a promising candidate for systemic delivery of PTX.

Optimization of PM Coating

To enhance the functionality of TPNs, PM coatings were applied to prepare PTPNs. PM coating provides immune evasion and tumor-targeting capabilities, improving the therapeutic potential of nanoparticles.[33] The stability of PTPNs was optimized by determining the appropriate PM/PLGA ratio. Several PTPNs were prepared at varying PM/PLGA ratios from 0.00125 to 0.02, and their stability was assessed by measuring particle size changes in PBS and rat plasma, which simulate physiological environments.

For uncoated TPNs (PM/PLGA ratio = 0), the particle size increased from 203 ± 1 nm in DW to 245 ± 3 nm in PBS, indicating aggregation due to ionic strength (Figure 2c). In contrast, PTPNs with PM/PLGA ratios of 0.00125 to 0.02 exhibited improved stability. At a ratio of 0.005, the particle size changed minimally from 221 ± 2 nm in DW to 234 ± 3 nm in PBS, corresponding to a size change rate of less than 10%. This indicated that a PM/PLGA ratio of 0.005 effectively prevented aggregation in PBS. Similarly, in rat plasma, the size of PTPNs with a ratio of 0.005 increased to 245 ± 3 nm, which was significantly smaller than the 362 ± 5 nm observed for PTPNs with a 0.0025 ratio. These results demonstrated that a PM/PLGA ratio of 0.005 provided the necessary stability for systemic administration.

The optimization of PM coating was also confirmed through TEM imaging (Figure 2d–g). PTPNs prepared at PM/PLGA ratios of 0, 0.0025, and 0.005 exhibited distinct morphological differences. At a ratio of 0.0025, PM appeared as clustered aggregates around the nanoparticles, indicating incomplete coating. However, at a ratio of 0.005, a uniform PM layer approximately 20 nm thick was observed, confirming successful coating. This uniform coating is crucial for achieving biomimetic properties and ensuring efficient tumor targeting.

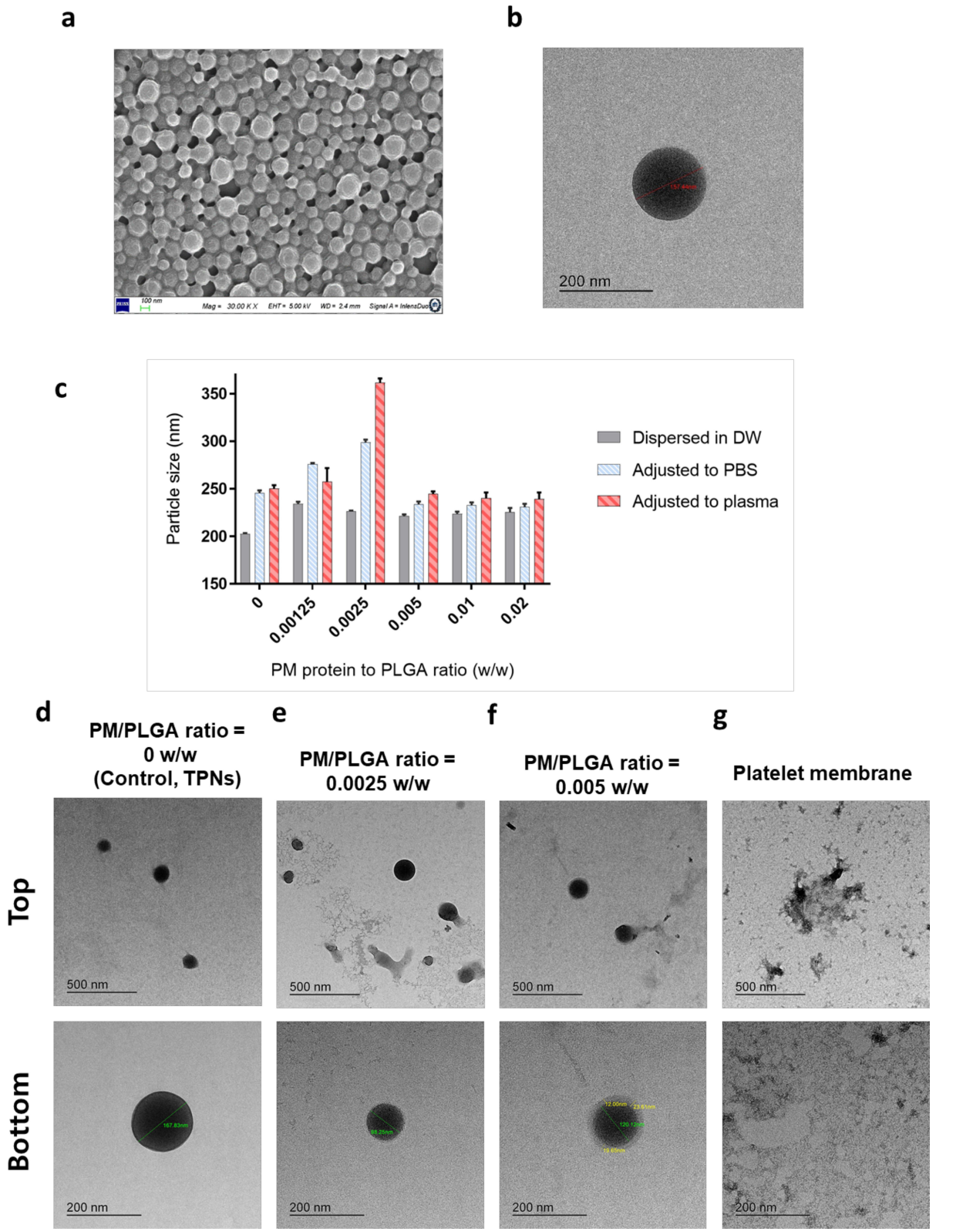

Figure 2 (**a**) SEM image of TPNs. (**b**) TEM image of TPNs. (**c**) Particle size change of PTPNs coated with varying PM to PLGA ratios (w/w) measured after dispersed in deionized water, after adjusting to PBS buffer solution, and after adjusting to plasma (n = 3). (**d–g**) TEM images of PTPNs at varying PM/ PLGA ratio (w/w): (**d**) 0 (control; TPNs); (**e**), 0.0025; (**f**), 0.005; (**g**) PM. The top is an image at low magnification, and the bottom is an image at high magnification.
Abbreviation: PM, Platelet membrane.

https://doi.org/10.2147/IJN.S517753

Characterization of PTPNs

The characterization of PTPNs were investigated through particle size, PDI, zeta potential measurements, Western blot analysis, and TEM imaging (Figure 3). The particle size of TPNs was measured as 203 ± 1 nm, while PTPNs exhibited a slightly increased size of 221 ± 2 nm, reflecting an 18 nm increase after PM coating (Figure 3a). This increase in particle size after coating was consistent with findings from previous studies, supporting the conclusion that the PM successfully coated the TPNs.[23,34] The PDI values were 0.088 ± 0.013 for TPNs and 0.090 ± 0.020 for PTPNs, indicating narrow size distributions for both formulations. For zeta potential, TPNs exhibited a value of −16.0 ± 1.5 mV, while PTPNs showed a more negative value of −30.5 ± 0.3 mV, closely aligning with the zeta potential of PM, measured at −32.9 ± 1.5 mV (Figure 3a). This similarity in zeta potential between PTPNs and PM confirmed the successful coating of PM onto PTPNs, in accordance with previously reported characteristics of PM-based nanoparticles.[17,19] To further assess the physical robustness of the PTPNs, colloidal stability was monitored over 14 days in both PBS and 50% mouse plasma at 37°C. The particle size showed only modest increases (from 219 to 237 nm in PBS and from 225 to 256 nm in plasma), and the zeta potential remained relatively stable (from –30.7 to –29.3 mV in PBS and –29.8 to –27.7 mV in

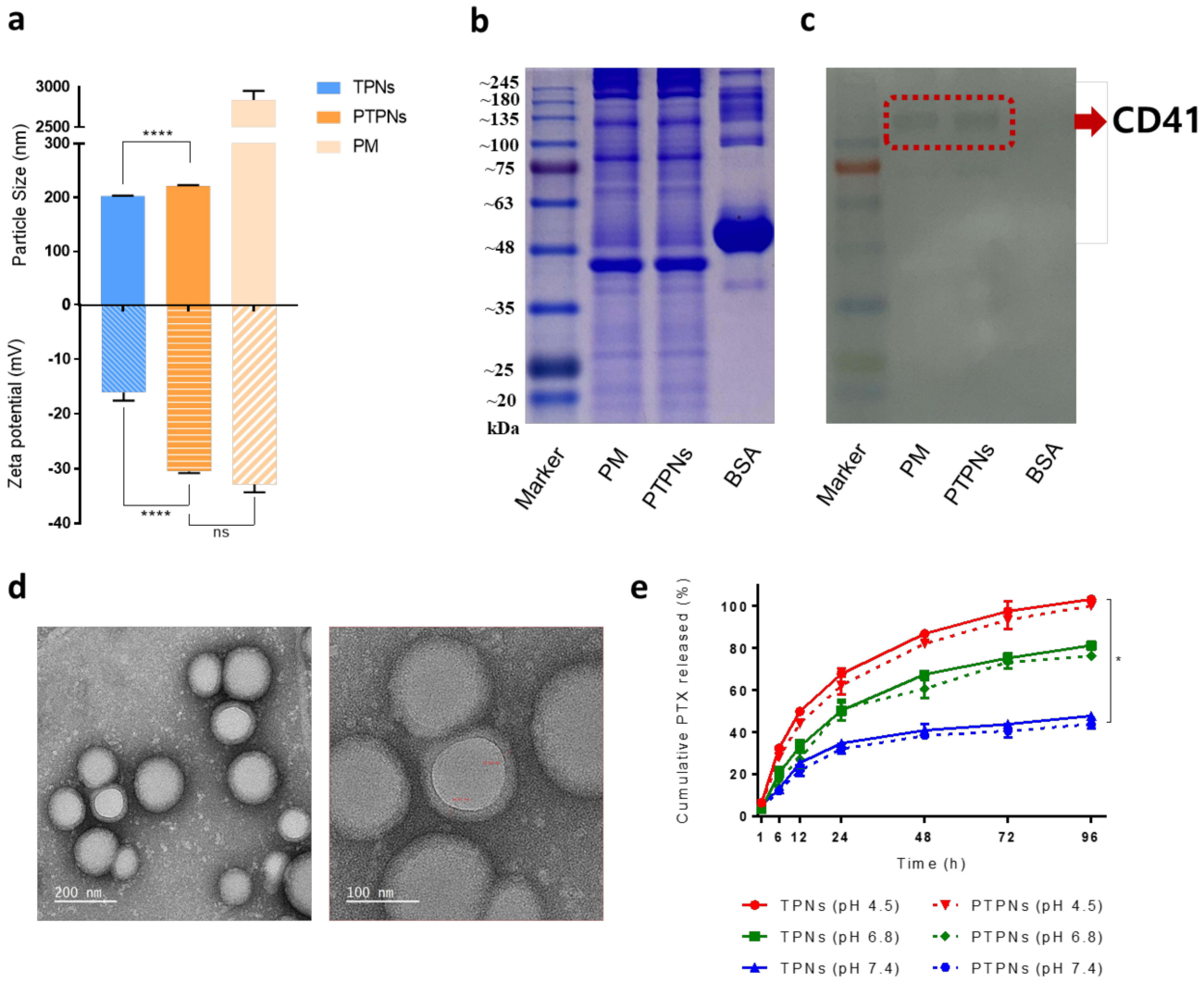

Figure 3 Characterization of PTPNs. (**a**) Particle size and zeta potential of TPNs, PTPNs, and PM (n = 3). (**b**) protein contents of PM, TPNs, and bovine serum albumin (BSA) visualized on a Coomassie blue stained SDS-PAGE gel. (**c**) Western blot analysis presenting CD41 protein bands in PM and PTPNs. BSA was used as a negative control. (**d**) TEM images of optimized PTPNs negatively stained with uranyl acetate. Left image: scale bar = 200 nm; right image: scale bar = 100 nm. (**e**) In vitro release profiles of PTX from TPNs and PTPNs: A, the cumulative released% of PTX from TPNs and PTPNs for 96 h in pH 4.5, 6.8, 7.4 buffer with 2% SDS (n = 3). *p* values: **p* < 0.05, *****p* < 0.0001.

Abbreviation: ns, not significant.

plasma), indicating good colloidal stability under both storage and physiologically relevant conditions (Supporting Information 3). Hemocompatibility of PTPNs was also evaluated by measuring hemolysis after 3 h incubation with red blood cells. The hemolysis percentage increased in a concentration-dependent manner, ranging from 0.1 ± 0.1% at 0 μg/mL to 3.5 ± 0.5% at 200 μg/mL. All values remained below the 5% threshold, which is commonly used as a criterion for acceptable blood compatibility (Supporting Information 4). Platelet-mimicking systems have been increasingly explored for drug delivery applications due to their ability to evade immune detection and prolong circulation, which is critical for improving therapeutic efficacy, particularly against multidrug-resistant tumors.[4,17,20] The purification of PM was further validated through Western blot analysis by detecting CD41, a known protein marker for PM. A distinct CD41-specific band was observed in both PM and PTPNs, indicating that PM was successfully purified and coated on the TPNs (Figure 3b and c). Finally, the PTPNs were negatively stained with uranyl acetate and observed using TEM. A membrane structure approximately 15 nm thick was visualized, providing additional confirmation (Figure 3d–g). This membrane is presumed to have formed through spontaneous fusion of PM vesicles onto the surface of TPNs. The coating likely occurred via hydrophobic interactions and membrane fluidity–driven self-assembly, as described in previous studies on PM–based nanocarriers.[15,23] Additionally, recent studies suggest the significance of functional platelet proteins on the nanoparticle surface, which contribute to enhanced targeting of circulating tumor cells and tumor microenvironments.[19,20] This approach enables the nanoparticles to acquire surface proteins from platelets, which contribute to prolonged circulation, immune evasion, and potentially improved therapeutic outcomes, particularly for challenging cancers such as triple-negative breast cancer.[8]

An in vitro release study was conducted to evaluate the release profile of PTX from TPNs and PTPNs (Figure 3e). The cumulative release percentage of PTX from TPNs in pH 4.5 buffer reached 103% over 96 h, suggesting complete drug release. In pH 6.8 buffer, the release percentage was 81%, while in pH 7.4 buffer, it was 48%, reflecting a pH-dependent release behavior. Similarly, the cumulative release percentage of PTX from PTPNs in pH 4.5 buffer was 100% over 96 h. In pH 6.8 buffer, the release percentage was 76%, whereas in pH 7.4 buffer, it was 44%. This trend in release rates before and after PM coating is consistent with findings from previous studies.[35–38] Each pH condition represents a specific biological environment: the acidic lysosomal environment after cellular uptake (pH 4.5),[39] the slightly acidic tumor microenvironment (pH 6.8),[40] and the neutral physiological environment (pH 7.4).[41] Drug release was faster in acidic conditions, which is attributed to the carboxylic acid end group of PLGA.[42] In acidic environments, this group is protonated, accelerating polymer degradation and facilitating drug release. These results emphasize the controlled and pH-sensitive release, enabling selective drug release in acidic tumor environments while maintaining stability under neutral conditions. This pH-responsive behavior minimizes systemic toxicity and enhances therapeutic efficacy by facilitating drug release at the tumor site and limiting it in healthy tissues, demonstrating significant potential for improving cancer treatment outcomes.[43–45] In addition, PTX release from PTPNs in 50% mouse plasma was evaluated to assess behavior under biologically relevant conditions. Compared to pH 5.5 buffer, which showed rapid release (98% over 96 h), plasma exhibited a more sustained pattern (81% over 96 h), which may be explained by protein interactions and the neutral pH environment (Supporting Information 5).

Cell Viability Study

Figure 4 demonstrates the cytotoxic effects of free PTX, B-TPNs, B-PTPNs, TPNs, and PTPNs on MCF-7 and MCF-7/ADR cells after 24 and 48 h of treatment. In MCF-7 cells, the IC_{50} values for free PTX, B-TPNs, TPNs, and PTPNs were measured as 3.1 μg/mL, 465.3 μg/mL, 253.7 μg/mL, 13.5 μg/mL, and 5.0 μg/mL, respectively, at 24 h. After 48 h, these values decreased to 2.5 μg/mL, 313.3 μg/mL, 157.3 μg/mL, 3.0 μg/mL, and 1.6 μg/mL, respectively (Figure 4a and b). In MCF-7/ADR cells, which are known to exhibit resistance to PTX due to P-gp efflux, the IC_{50} values for free PTX were significantly higher, recorded at 78.9 μg/mL at 24 h and 46.8 μg/mL. Conversely, PTPNs displayed the lowest IC_{50} values in MCF-7/ADR cells at 3.8 μg/mL and 2.6 μg/mL after 24 and 48 h, respectively (Figure 4c and d). The higher IC_{50} values observed in MCF-7/ADR cells for free PTX reflect the role of P-gp efflux pumps in reducing intracellular drug accumulation.[46] Specifically, the IC_{50} of free PTX in MCF-7/ADR cells was 25.5-fold higher than in MCF-7 cells after 24 h and 18.9-fold higher after 48 h, demonstrating the extent of drug resistance. In contrast, TPNs and PTPNs, which incorporate TPGS as a P-gp inhibitor, significantly mitigated this resistance. The IC_{50} values for TPNs in MCF-7/

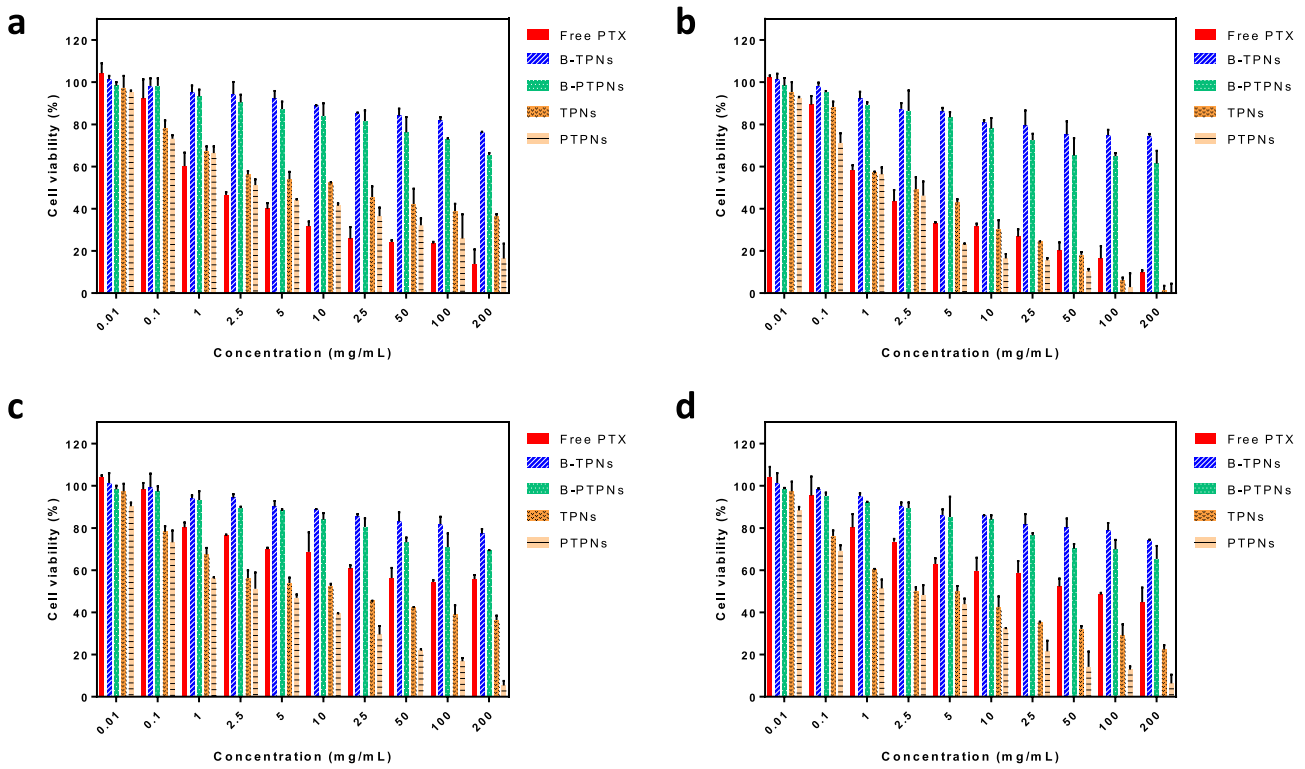

Figure 4 Cytotoxicity of B-TPNs, B-PTPNs, TPNs, and PTPNs compared to free PTX. Cell viability assays were conducted against MCF-7 cells for (**a**) 24 h and (**b**) 48 h, and against MCF-7/ADR cells for (**c**) 24 h and (**d**) 48 h (n = 5).

ADR cells were 1.5-fold higher than in MCF-7 cells after 24 h and slightly lower (0.8-fold) after 48 h, respectively. These findings are consistent with previous studies showing that TPGS effectively inhibits P-gp efflux, thereby enhancing intracellular drug retention.[47,48]

PTPNs also exhibited higher cytotoxicity compared to TPNs in all conditions, indicating enhanced targetability. This is attributed to the interaction between P-selectin on the PM surface and CD44 receptors overexpressed on tumor cells, promoting greater cellular uptake of the nanoparticles.[49] Recent advances also support the use of PM-coated nanoparticles to achieve targeted delivery and immune evasion, offering significant advantages for overcoming multidrug resistance.[17,19] Furthermore, the sustained drug release from the nanoparticles contributed to increased cytotoxicity after 48 h compared to 24 h, as the prolonged release ensured continuous drug exposure to the cells. Controlled and stimuli-responsive release profiles are increasingly recognized as key features for maintaining therapeutic drug concentrations within the tumor microenvironment and for overcoming resistance.[4]

Overall, these results emphasize that the combination of TPGS surface modification, PM coating, and sustained drug release effectively improves intracellular drug delivery, overcoming multidrug resistance mechanisms while enhancing the therapeutic efficacy of PTX. These findings support the potential application of PTPNs as a targeted and efficient drug delivery system for treating drug-resistant cancers.

Flow Cytometry

The cellular uptake of TPNs and PTPNs in MCF-7 and MCF-7/ADR cells was evaluated using C6 (coumarin 6) as a fluorescent probe instead of PTX. Intracellular fluorescence intensity, measured by flow cytometry at 2, 6, and 24 h (Figure 5), showed time-dependent differences in uptake for the various formulations. Free C6 exhibited the highest fluorescence intensity at early time points, but its intensity decreased over time due to rapid cellular metabolism and elimination. In contrast, C6-TPNs and C6-PTPNs demonstrated sustained and increasing fluorescence intensity, reflecting the controlled release properties of PLGA-based nanoparticles. At 2 and 6 h, free C6 showed the highest fluorescence intensity, followed by C6-PTPNs and C6-TPNs (Figure 5a and b). However, after 24 h, the ranking shifted,

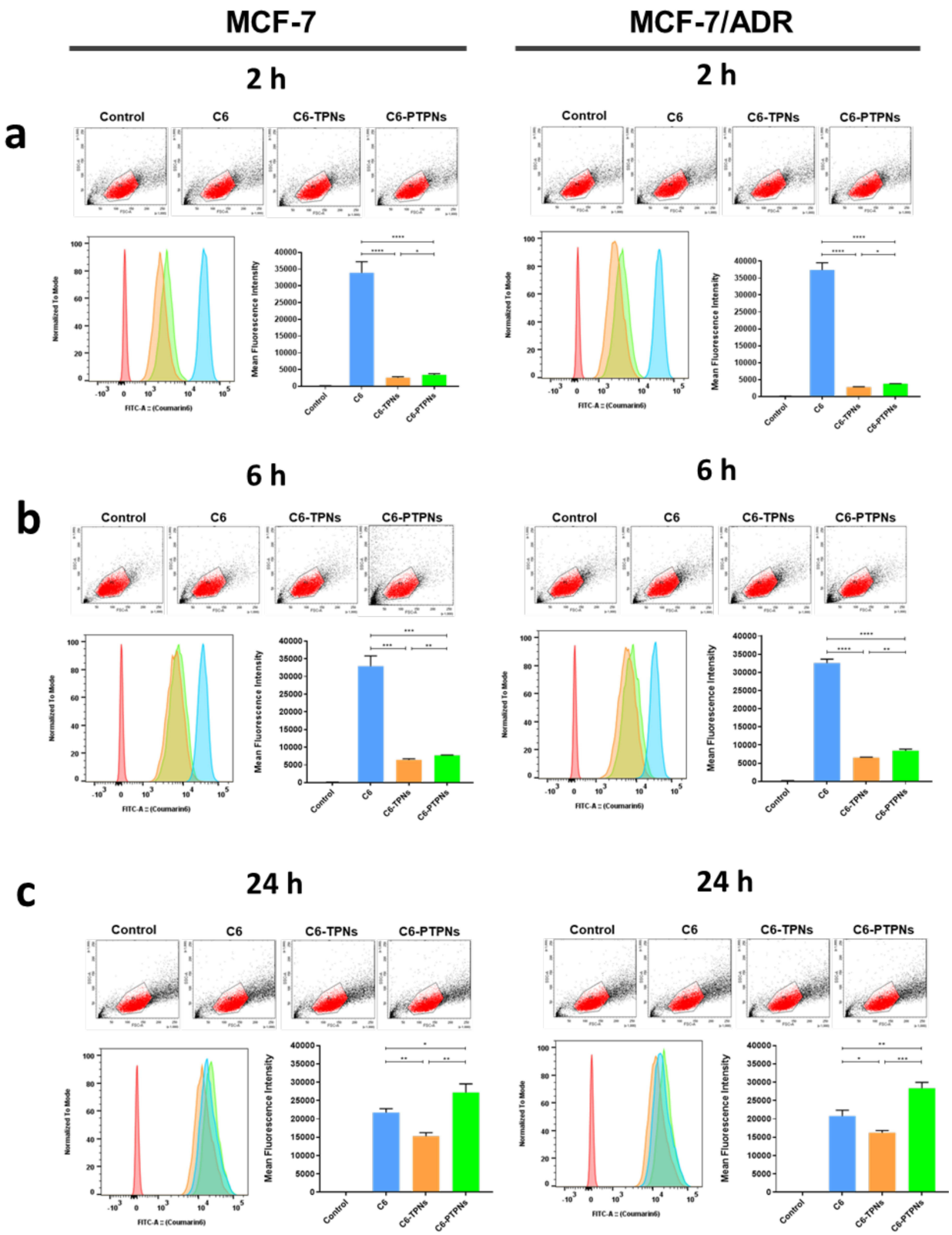

Figure 5 Cellular uptake of free C6, C6-TPNs, and C6-PTPNs in MCF-7 and MCF-7/ADR cells analyzed by flow cytometry at (**a**) 2 h, (**b**) 6 h, and (**c**) 24 h (n = 3). *p* values: **p* < 0.05, ***p* < 0.01, ****p* < 0.001, and *****p* < 0.0001.
Abbreviation: ns, not significant.

https://doi.org/10.2147/IJN.S517753

with C6-PTPNs exhibiting the highest fluorescence intensity, suggesting superior intracellular accumulation (Figure 5c). This improvement is attributed to the targeting capabilities of PTPNs, mediated by interactions between P-selectin on PM and CD44 receptors on cancer cells.[50] Recent studies have shown that PM-coated nanoparticles not only improve cellular uptake through receptor-mediated pathways but also enhance intracellular retention by evading lysosomal degradation and immune recognition.[4,19]

The gradual increase in fluorescence intensity of C6-TPNs and C6-PTPNs over time is consistent with their sustained release profiles, as confirmed in the in vitro PTX release study. Such prolonged intracellular fluorescence is in line with emerging evidence that sustained-release nanocarriers provide continuous payload delivery, which is advantageous for maintaining therapeutic levels in tumor cells over time.[4]

The difference in fluorescence intensity between MCF-7 and MCF-7/ADR cells was minimal for all formulations, because C6 is not a substrate for P-gp. However, the greater accumulation of C6-PTPNs compared to C6-TPNs emphasizes the role of PM coating in enhancing cellular uptake. These results are consistent with previous studies showing that receptor-mediated endocytosis plays an important role in nanoparticle internalization.

In summary, PLGA nanoparticles, particularly PTPNs, effectively maintain intracellular drug delivery. The integration of PM targeting and sustained delivery is increasingly recognized as a promising strategy for enhancing selective uptake and therapeutic retention in drug-resistant tumor cells.[4,20] The combination of controlled release, surface modification with PTGS, and PM coating minimizes metabolic clearance while enhancing drug retention in cancer cells. This approach improves therapeutic efficiency and demonstrates potential for overcoming drug resistance in cancer treatment.

In vivo Distribution

Cy5.5 fluorescent dye was encapsulated in TPNs and PTPNs to investigate their biodistribution in tumors and major organs (Figure 6). Free Cy5.5, Cy5.5-TPNs, and Cy5.5-PTPNs were injected via the tail vein into BALB/c nude mice bearing MCF-7/ADR tumors, and their distribution was investigated. The tumor location, marked by a red dotted line in Figure 6a, showed no fluorescence in the untreated control group. In the free Cy5.5 group, minimal fluorescence was observed at the tumor site, indicating poor delivery efficiency. Most of the dye accumulated in other organs and was quickly cleared. For the Cy5.5-TPNs group, strong fluorescence was detected in the abdominal area containing major organs within 2 h of injection, but no accumulation was seen at the tumor site. By 24 h, fluorescence intensity diminished significantly, localizing primarily in the liver (Figure 6b).

In contrast, the Cy5.5-PTPNs group showed high fluorescence in the abdominal area within 2 h, with noticeable accumulation at the tumor site. Over time, fluorescence intensity at the tumor remained stable or increased, demonstrating effective targeting. After 24 h, mice were sacrificed, and fluorescence intensities were measured in tumors and major organs, including the liver, heart, spleen, lungs, and kidneys (Figure 6b and c). Cy5.5-PTPNs exhibited significant tumor accumulation, with fluorescence intensity comparable to that observed in the spleen, lungs, and kidneys, confirming their tumor-targeting capability. These findings indicate that the PM coating on PTPNs contributes to tumor-specific accumulation, a result that is in agreement with recent studies reporting enhanced biodistribution and immune evasion of PM-coated nanoparticles through interactions with tumor-associated receptors.[17,19,20]

Although PTPNs exhibited a particle size greater than 200 nm, which may increase the likelihood of macrophage uptake, fluorescence imaging showed limited accumulation in liver and spleen, suggesting minimal interaction with the mononuclear phagocyte system. While these results provide indirect evidence of Reticuloendothelial system (RES) evasion, additional studies are planned to directly assess macrophage uptake using in vitro and in vivo methods.

In vivo Antitumor Activity Study

The anticancer efficacy of PTX in various formulations was evaluated in BALB/c nude mice bearing MCF-7/ADR tumors. TPNs, PTPNs, and the PTX commercial product were administered intravenously every 3 days, and tumor volume and body weight were monitored over 14 days (Figure 7a and b). The red dashed lines indicate the PTX injection time points. As shown in Figure 7a, tumor volume increased by 299% in the PBS control group after 14 days. In comparison, the tumor volume increased by 221% in the PTX commercial product group, 246% in the TPNs group, and

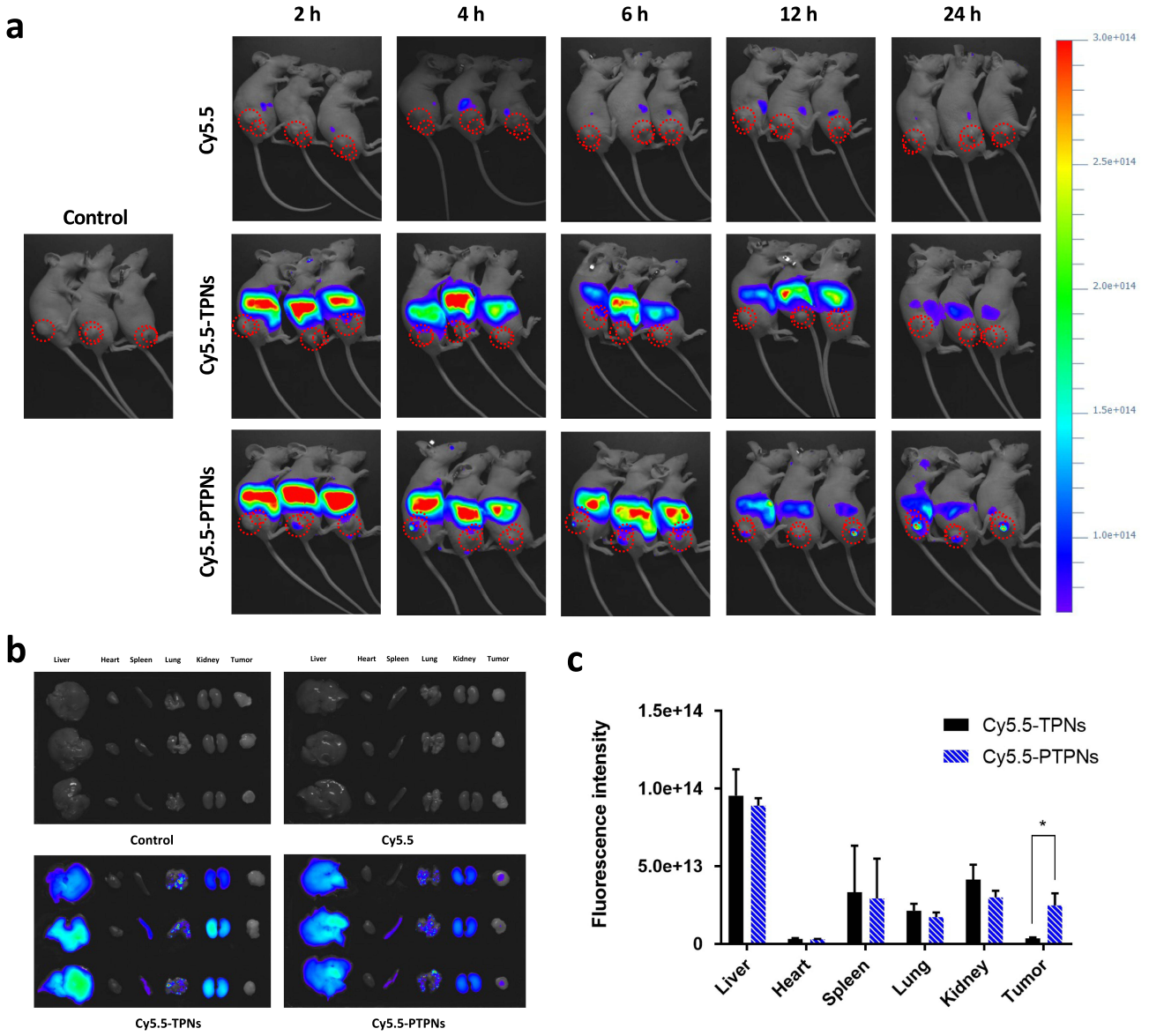

Figure 6 In vivo and ex vivo imaging of free Cy5.5, Cy5.5-TPNs, and Cy5.5-PTPNs in nude mice bearing MCF-7/ADR tumors. (**a**) Fluorescence images captured at various time points up to 24 following intravenous injection (n = 3). Red dashed line indicates the xenografted tumor tissue in mice. (**b**) Ex vivo fluorescence images of tumors and major organs 24 h post-injection. (**c**) Quantitative analysis of fluorescence intensities in tumors and major organs (n = 3). *p* values: **p* < 0.05.
Abbreviation: ns, not significant.

161% in the PTPNs group. PTPNs demonstrated significantly enhanced tumor growth inhibition compared to both TPNs and PTX commercial product. This enhanced efficacy can be attributed to the tumor-targeting effect of the PM coating, as supported by the biodistribution data. Recent research indicates that PM -coated carriers may also influence the tumor microenvironment by reducing immunosuppressive interactions, thereby contributing to improved therapeutic responses.[17,19]

Figure 7b illustrates body weight changes to assess the side effects of the formulations. The PBS group showed a 107% increase in body weight after 14 days, reflecting tumor and natural body growth in the mice. Conversely, the PTX commercial product group exhibited a 98% body weight change. TPNs and PTPNs maintained body weight at 104% and 101%, respectively, after 14 days, suggesting that the PLGA, PVA, TPGS, and PM components appear to be well tolerated at the tested dose, without inducing significant observable toxicity during the study period.

https://doi.org/10.2147/IJN.S517753

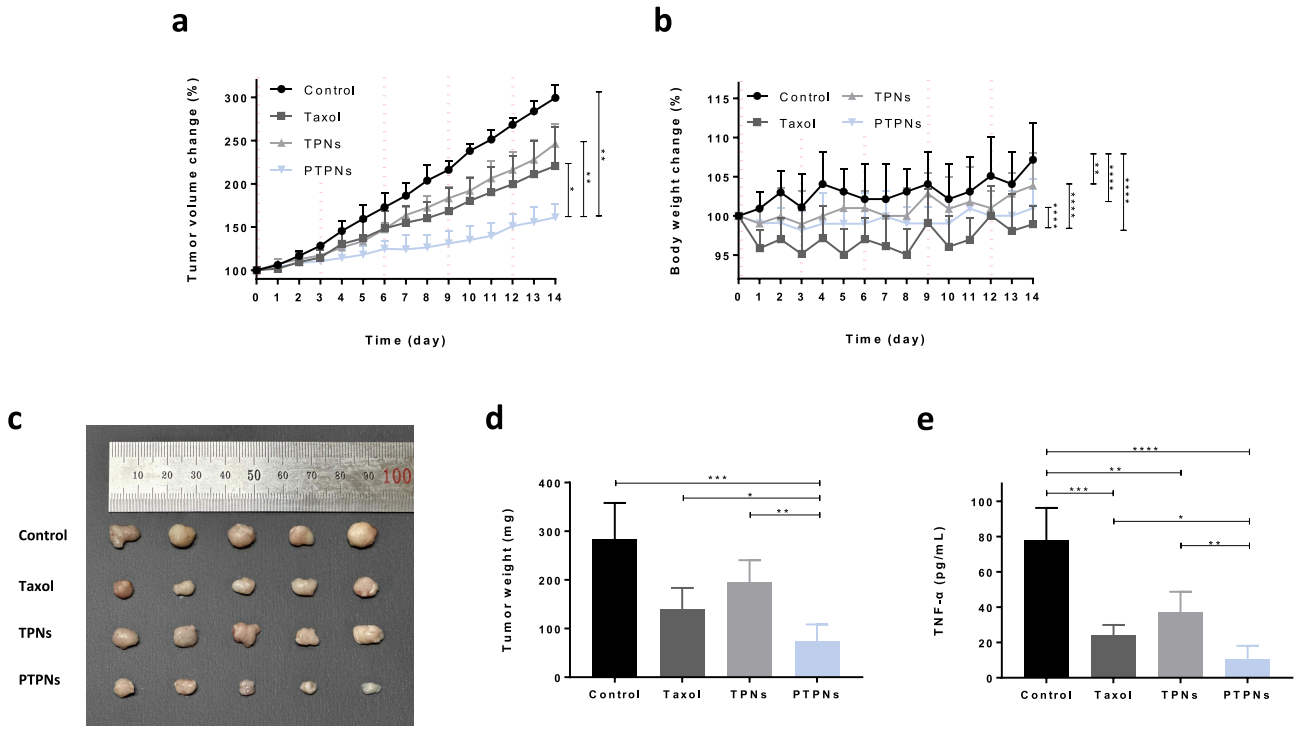

Figure 7 In vivo antitumor efficacy of control (PBS), PTX commercial product (Taxol®), TPNs, and PTPNs in nude mice bearing MCF-7/ADR tumors. (**a**) Tumor growth curves according to volume changes over 14 days, with formulations administered intravenously every 3 days (red dashed lines indicate injection time points) (n =5). (**b**) Body weight changes of mice in each experimental group during the treatment period (n =5). (**c**) Representative images of tumors excised from mice after 14 days of treatment. (**d**) Average tumor weights recorded from the excised tumors after 14 days of treatment (n =5). (**e**) TNF-α levels in serum after 14 days of treatment (n = 5). *p* values: **p* < 0.05, ***p* < 0.01, ****p* < 0.001, *****p* < 0.0001 (mean ± SD; n = 5).
Abbreviation: ns, not significant.

Tumor tissues excised after 14 days of treatment (Figure 7c and d) confirmed the therapeutic outcomes. The measured tumor volumes were 509 mm^3 (control), 264 mm^3 (PTX commercial product), 418 mm^3 (TPNs), and 196 mm^3 (PTPNs), while the corresponding tumor weights were 283 mg, 139 mg, 195 mg, and 75 mg, respectively. PTPNs showed significant reductions in both tumor size and weight compared to all other groups.

The effect of TNF-α, a cytokine linked to tumor progression, was also evaluated after days (Figure 7e). TNF-α levels in serum were 75.0 pg/mL (PBS; control), 24.3 pg/mL (PTX commercial product), 37.0 pg/mL (TPNs), and 10.4 pg/mL (PTPNs). The TNF-α levels correlated with tumor volume and weight, with PTPNs showing the lowest concentration: 7.2-fold lower than control, 3.6-fold lower than TPNs, and 2.3-fold lower than PTX commercial product. These findings indicate that the PM coating enhances tumor suppression by reducing TNF-α, which promotes cell survival and tumor growth via nuclear factor kappa B- (NFκB-), phosphoinositide-3-kinase–protein kinase B/Akt – (PI3K-PKB/Akt-), and mitogen-activated protein kinase– (MAPK-) dependent pathways.[51]

Some studies have proposed that high concentrations of TNF-α (2000–8500 ng/mL) may exert anti-tumor effects by inducing apoptosis and triggering immune-mediated tumor destruction.[52,53] However, the TNF-α levels observed in this study (<100 pg/mL) are far below this threshold and indicate that TNF-α primarily acted as a tumor-promoting factor.[54,55] At these lower concentrations, TNF-α is known to contribute to tumor progression by promoting cell survival, proliferation, and angiogenesis through the activation of NFκB-, PI3K-PKB/Akt-, and MAPK-dependent signaling pathways.[56,57] Nanoparticle systems with sustained release profiles have been shown to gradually attenuate pro-inflammatory cytokines such as TNF-α, supporting long-term suppression of tumor-promoting pathways.[4,20] This dual role of TNF-α, as both a tumor promoter at lower levels and a potential anti-tumor agent at higher levels, indicates the complexity of its biological functions and highlights the importance of context-dependent modulation.

The findings of this study demonstrate that PTPNs effectively reduce TNF-α levels in the tumor microenvironment, resulting in significant inhibition of tumor growth. By minimizing systemic side effects while targeting tumor-promoting

factors, PTPNs present a promising strategy for enhancing therapeutic efficacy in cancer treatment. Collectively, the findings support the use of PTPNs as an effective platform for targeted chemotherapy and suggest a broader utility in addressing drug-resistant cancers by modulating inflammatory signaling and improving nanoparticle–tumor interactions.

Conclusion

This study presents the development of PTPNs as a tumor-targeted drug delivery system with potential application in the treatment of drug-resistant cancers. The nanoparticles were successfully prepared and thoroughly characterized by particle size measurements, TEM, and Western blot analysis, confirming the presence of a functional PM coating. The resulting formulation exhibited pH-sensitive drug release, improved intracellular uptake, and enhanced cytotoxic effects against both drug-sensitive and multidrug-resistant breast cancer cells. Furthermore, in vivo biodistribution analysis revealed preferential accumulation of PTPNs at tumor sites with limited off-target distribution. These findings support the utility of PM camouflage, TPGS-mediated efflux inhibition, and sustained release properties as complementary strategies for improving the precision and efficacy of PTX delivery.

Nevertheless, several limitations should be noted. The in vivo evaluation was limited to a single xenograft model and did not include orthotopic or metastatic tumor models, which may better reflect the clinical complexity of drug-resistant cancers. Biodistribution analysis relied on a fluorescent surrogate rather than direct quantification of PTX, and long-term pharmacokinetics, toxicity, and immunogenicity were not assessed. Additional preclinical studies incorporating various tumor types, drug quantification, and systemic safety evaluations will be essential to support clinical translation.

In summary, the PTPNs developed in this study represent a promising nanoparticle platform for targeted chemotherapy. By combining biomimetic targeting, intracellular retention, and controlled drug release, this system offers a strategic solution for overcoming multidrug resistance and improving therapeutic selectivity. The findings provide a rational basis for further development of PM–based nanotherapeutics aimed at enhancing treatment outcomes in cancer and other pathologies requiring targeted drug delivery. Future studies will focus on evaluating therapeutic efficacy in orthotopic and metastatic tumor models, performing quantitative biodistribution using the active drug, and assessing long-term pharmacokinetics and safety to facilitate clinical translation.

Acknowledgment

B.S Song, Y.G Na and B.J Kim contributed equally to this work. This work was supported by the National Research Foundation of Korea (NRF) grant funded by the Korea government (MSIT) (RS-2024-00455804).

Disclosure

The authors declare no conflicts of interest in this work.

References

1. Abu Samaan TM, Samec M, Liskova A, Kubatka P, Büsselberg D. Paclitaxel's mechanistic and clinical effects on breast cancer. *Biomolecules*. 2019;9(12):789. doi:10.3390/biom9120789
2. Alalawy AI. Key genes and molecular mechanisms related to paclitaxel resistance. *Cancer Cell Int*. 2024;24(1):244. doi:10.1186/s12935-024-03415-0
3. Callaghan R, Luk F, Bebawy M. Inhibition of the multidrug resistance P-glycoprotein: time for a change of strategy? *Drug Metab Dispos*. 2014;42(4):623–631. doi:10.1124/dmd.113.056176
4. Duan C, Yu M, Xu J, Li BY, Zhao Y, Kankala RK. Overcoming cancer multi-drug resistance (MDR): reasons, mechanisms, nanotherapeutic solutions, and challenges. *Biomed Pharmacother*. 2023;162:114643. doi:10.1016/j.biopha.2023.114643
5. Gelderblom H, Verweij J, Nooter K, Sparreboom A. Cremophor EL: the drawbacks and advantages of vehicle selection for drug formulation. *Eur J Cancer*. 2001;37(13):1590–1598. doi:10.1016/S0959-8049(01)00171-X
6. Bernabeu E, Cagel M, Lagomarsino E, Moretton M, Chiappetta DA. Paclitaxel: what has been done and the challenges remain ahead. *Int J Pharm*. 2017;526(1–2):474–495. doi:10.1016/j.ijpharm.2017.05.016
7. Dinarvand R, Sepehri N, Manoochehri S, Rouhani H, Atyabi F. Polylactide-co-glycolide nanoparticles for controlled delivery of anticancer agents. *Int J Nanomed*. 2011;6:877–895. doi:10.2147/IJN.S18905
8. Dinakar YH, Rajana N, Kumari NU, Jain V, Mehra NK. Recent advances of multifunctional PLGA nanocarriers in the management of triple-negative breast cancer. *AAPS Pharm Sci Tech*. 2023;24(8):258. doi:10.1208/s12249-023-02712-7
9. Makadia HK, Siegel SJ. Poly lactic-co-glycolic acid (PLGA) as biodegradable controlled drug delivery carrier. *Polymers*. 2011;3(3):1377–1397. doi:10.3390/polym3031377

10. Mehta P, Shende P. Evasion of opsonization of macromolecules using novel surface-modification and biological-camouflage-mediated techniques for next-generation drug delivery. *Cell Biochem Funct*. 2023;41(8):1031–1043. doi:10.1002/cbf.3880
11. Owens DE, Peppas NA. Opsonization, biodistribution, and pharmacokinetics of polymeric nanoparticles. *Int J Pharm*. 2006;307(1):93–102. doi:10.1016/j.ijpharm.2005.10.010
12. Luiz MT, Di Filippo LD, Alves RC, et al. The use of TPGS in drug delivery systems to overcome biological barriers. *Eur Polym J*. 2021;142:110129. doi:10.1016/j.eurpolymj.2020.110129
13. Sun Y, Yu B, Wang G, et al. Enhanced antitumor efficacy of vitamin E TPGS-emulsified PLGA nanoparticles for delivery of paclitaxel. *Colloids Surf B Biointerfaces*. 2014;123:716–723. doi:10.1016/j.colsurfb.2014.10.007
14. Liu BY, Wu C, He XY, Zhuo RX, Cheng SX. Multi-drug loaded vitamin E-TPGS nanoparticles for synergistic drug delivery to overcome drug resistance in tumor treatment. *Sci Bull*. 2016;61(7):552–560. doi:10.1007/s11434-016-1039-5
15. Han H, Bartolo R, Li J, Shahbazi MA, Santos HA. Biomimetic platelet membrane-coated nanoparticles for targeted therapy. *Eur J Pharm Biopharm*. 2022;172:1–15. doi:10.1016/j.ejpb.2022.01.004
16. Bang KH, Na YG, Huh HW, et al. The delivery strategy of paclitaxel nanostructured lipid carrier coated with platelet membrane. *Cancers*. 2019;11(6):807. doi:10.3390/cancers11060807
17. Safdar A, Wang P, Muhaymin A, Nie G, Li S. From bench to bedside: platelet biomimetic nanoparticles as a promising carriers for personalized drug delivery. *J Control Release*. 2024;373:128–144. doi:10.1016/j.jconrel.2024.07.013
18. Zeng Y, Li S, Zhang S, Wang L, Yuan H, Hu F. Cell membrane coated-nanoparticles for cancer immunotherapy. *Acta Pharm Sin B*. 2022;12(8):3233–3254. doi:10.1016/j.apsb.2022.02.023
19. Yang L, Zhang K, Zheng D, et al. Platelet-based nanoparticles with stimuli-responsive for anti-tumor therapy. *Int J Nanomed*. 2023;18:6293–6309. doi:10.2147/IJN.S436373
20. Tang M, Zhang Z, Wang P, et al. Advancements in precision nanomedicine design targeting the anoikis-platelet interface of circulating tumor cells. *Acta Pharm Sin B*. 2024;14(8):3457–3475. doi:10.1016/j.apsb.2024.04.034
21. Na YG, Pham TMA, Byeon JJ, et al. Development and evaluation of TPGS/PVA-based nanosuspension for enhancing dissolution and oral bioavailability of ticagrelor. *Int J Pharm*. 2020;586:119287. doi:10.1016/j.ijpharm.2020.119287
22. Hu CMJ, Fang RH, Wang KC, et al. Nanoparticle biointerfacing by platelet membrane cloaking. *Nature*. 2015;526(7571):118–121. doi:10.1038/nature15373
23. Wei X, Gao J, Fang RH, et al. Nanoparticles camouflaged in platelet membrane coating as an antibody decoy for the treatment of immune thrombocytopenia. *Biomaterials*. 2016;111:116–123. doi:10.1016/j.biomaterials.2016.10.003
24. Paul A, Straub A, Weber N, Ziemer G, Wendel HP. CD41 western blotting: a new method to detect platelet adhesion to artificial surfaces used in extracorporeal circulation procedures. *J Mater Sci Mater Med*. 2009;20:373–378. doi:10.1007/s10856-008-3587-y
25. Na YG, Huh HW, Kim MK, et al. Development and evaluation of a film-forming system hybridized with econazole-loaded nanostructured lipid carriers for enhanced antifungal activity against dermatophytes. *Acta Biomater*. 2020;101:507–518. doi:10.1016/j.actbio.2019.10.024
26. Kim HE, Na YG, Jin M, et al. Fabrication and evaluation of chitosan-coated nanostructured lipid carriers for co-delivery of paclitaxel and PD-L1 siRNA. *Int J Pharm*. 2024;666:124835. doi:10.1016/j.ijpharm.2023.124835
27. Fleming JM, Miller TC, Meyer MJ, Ginsburg E, Vonderhaar BK. Local regulation of human breast xenograft models. *J Cell Physiol*. 2010;224(3):795–806. doi:10.1002/jcp.22190
28. Jin M, Cho HJ, Na YG, et al. Practical approach to development of GS-445124-loaded PLGA nanoparticles for the long-term treatment of feline infectious peritonitis caused by feline coronavirus infection. *Int J Pharm*. 2025;674:125468. doi:10.1016/j.ijpharm.2024.125468
29. Börgermann J, Friedrich I, Flohe S, et al. Tumor necrosis factor-α production in whole blood after cardiopulmonary bypass: downregulation caused by circulating cytokine-inhibitory activities. *J Thorac Cardiovasc Surg*. 2002;124(3):608–617. doi:10.1067/mtc.2002.122300
30. Nakamura Y, Mochida A, Choyke PL, Kobayashi H. Nanodrug delivery: is the enhanced permeability and retention effect sufficient for curing cancer? *Bioconjug Chem*. 2016;27(10):2225–2238. doi:10.1021/acs.bioconjchem.6b00437
31. Wang G, Yu B, Wu Y, Huang B, Yuan Y, Liu CS. Controlled preparation and antitumor efficacy of vitamin E TPGS-functionalized PLGA nanoparticles for delivery of paclitaxel. *Int J Pharm*. 2013;446(1–2):24–33. doi:10.1016/j.ijpharm.2013.02.004
32. Mourdikoudis S, Pallares RM, Thanh NT. Characterization techniques for nanoparticles: comparison and complementarity upon studying nanoparticle properties. *Nanoscale*. 2018;10(27):12871–12934. doi:10.1039/C8NR02278J
33. Liu L, Pan D, Chen S, et al. Systematic design of cell membrane coating to improve tumor targeting of nanoparticles. *Nat Commun*. 2022;13(1):6181. doi:10.1038/s41467-022-33829-3
34. Li B, Chu T, Wei J, et al. Platelet-membrane-coated nanoparticles enable vascular disrupting agent combining anti-angiogenic drug for improved tumor vessel impairment. *Nano Lett*. 2021;21(6):2588–2595. doi:10.1021/acs.nanolett.1c00168
35. Hu Q, Sun W, Qian C, Wang C, Bomba HN, Gu Z. Anticancer platelet-mimicking nanovehicles. *Adv Mater*. 2015;27(44):7043–7050. doi:10.1002/adma.201503323
36. Pei W, Huang B, Chen S, Wang L, Xu Y, Niu C. Platelet-mimicking drug delivery nanoparticles for enhanced chemo-photothermal therapy of breast cancer. *Int J Nanomed*. 2020;15:10151–10167. doi:10.2147/IJN.S285952
37. Zhao C, Chen Q, Li W, Zhang J, Yang C, Chen D. Multi-functional platelet membrane-camouflaged nanoparticles reduce neuronal apoptosis and regulate microglial phenotype during ischemic injury. *Appl Mater Today*. 2022;27:101412. doi:10.1016/j.apmt.2022.101412
38. Jiang H, Tang C, Wen Y, et al. Enhanced antitumor efficacy of novel biomimetic platelet membrane-coated tetrandrine nanoparticles in nonsmall cell lung cancer. *Mol Pharm*. 2023;20(11):5463–5475. doi:10.1021/acs.molpharmaceut.3c00310
39. Zeng J, Shirihai OS, Grinstaff MW. Modulating lysosomal pH: a molecular and nanoscale materials design perspective. *J Life Sci*. 2020;2(4):25–37. doi:10.36069/jols/20201204
40. Lee S, Shanti A. Effect of exogenous pH on cell growth of breast cancer cells. *Int J Mol Sci*. 2021;22(18):9910. doi:10.3390/ijms22189910
41. Schwalfenberg GK. The alkaline diet: is there evidence that an alkaline pH diet benefits health? *J Environ Public Health*. 2012;2012:727630. doi:10.1155/2012/727630
42. Yoo JW, Mitragotri S. Polymer particles that switch shape in response to a stimulus. *Proc Natl Acad Sci U S A*. 2010;107(25):11205–11210. doi:10.1073/pnas.1000346107

43. Singh J, Nayak P. pH-responsive polymers for drug delivery: trends and opportunities. *J Polym Sci*. 2023;61(22):2828–2850. doi:10.1002/pol.20230403
44. He Q, Chen J, Yan J, et al. Tumor microenvironment responsive drug delivery systems. *Asian J Pharm Sci*. 2020;15(4):416–448. doi:10.1016/j.ajps.2019.04.003
45. Liu Y, Wang W, Yang J, Zhou C, Sun J. pH-sensitive polymeric micelles triggered drug release for extracellular and intracellular drug targeting delivery. *Asian J Pharm Sci*. 2013;8(3):159–167. doi:10.1016/j.ajps.2013.07.021
46. Liu Y, Zhou C, Wei S, et al. Paclitaxel delivered by CD44 receptor-targeting and endosomal pH-sensitive dual functionalized hyaluronic acid micelles for multidrug resistance reversion. *Colloids Surf B Biointerfaces*. 2018;170:330–340. doi:10.1016/j.colsurfb.2018.06.024
47. Win KY, Feng SS. In vitro and in vivo studies on vitamin E TPGS-emulsified poly(d,l-lactic-co-glycolic acid) nanoparticles for paclitaxel formulation. *Biomaterials*. 2006;27(10):2285–2291. doi:10.1016/j.biomaterials.2005.11.008
48. Kim CH, Kim BD, Lee TH, et al. Synergistic co-administration of docetaxel and curcumin to chemoresistant cancer cells using PEGylated and RIPL peptide-conjugated nanostructured lipid carriers. *Cancer Nanotechnol*. 2022;13(1):17. doi:10.1186/s12645-022-00119-w
49. Wang H, Wu J, Williams GR, et al. Platelet-membrane-biomimetic nanoparticles for targeted antitumor drug delivery. *J Nanobiotechnology*. 2019;17(1):60. doi:10.1186/s12951-019-0494-y
50. Elaskalani O, Berndt MC, Falasca M, Metharom P. Targeting platelets for the treatment of cancer. *Cancers*. 2017;9(7):94. doi:10.3390/cancers9070094
51. He Y, Sun MM, Zhang GG, et al. Targeting PI3K/Akt signal transduction for cancer therapy. *Signal Transduct Target Ther*. 2021;6(1):425. doi:10.1038/s41392-021-00828-5
52. Posner MC, Lienard D, Lejeune FJ, Rosenfelder D, Kirkwood J. Hyperthermic isolated limb perfusion with tumor necrosis factor alone for melanoma. *Cancer J Sci Am*. 1995;1(4):274–280.
53. Montfort A, Colacios C, Levade T, Andrieu-Abadie N, Meyer N, Ségui B. The TNF paradox in cancer progression and immunotherapy. *Front Immunol*. 2019;10:1818. doi:10.3389/fimmu.2019.01818
54. Wang X, Lin Y. Tumor necrosis factor and cancer, buddies or foes? *Acta Pharmacol Sin*. 2008;29(11):1275–1288. doi:10.1111/j.1745-7254.2008.00889.x
55. Cai X, Cao C, Li J, et al. Inflammatory factor TNF-α promotes the growth of breast cancer via the positive feedback loop of TNFR1/NF-κB (and/or p38)/p-STAT3/HBXIP/TNFR1. *Oncotarget*. 2017;8(35):58338–58352. doi:10.18632/oncotarget.16873
56. Wu YD, Zhou B. TNF-α/NF-κB/Snail pathway in cancer cell migration and invasion. *Br J Cancer*. 2010;102(4):639–644. doi:10.1038/sj.bjc.6605530
57. Pavitra E, Kancharla J, Gupta VK, et al. The role of NF-κB in breast cancer initiation, growth, metastasis, and resistance to chemotherapy. *Biomed Pharmacother*. 2023;163:114822. doi:10.1016/j.biopha.2023.114822